JOURNAL OF CATALYSIS 156, 255–264 (1995)

Bifunctional Mechanism of Pyridine Hydrodenitrogenation

J. A. Marzari, S. Rajagopal, and R. Miranda[1]

Department of Chemical Engineering, University of Louisville, Louisville, Kentucky 40292

Received March 8, 1994; revised April 27, 1995; accepted June 23, 1995

The role of Mo coordinatively unsaturated sites (CUS) and Brønsted acidic sites in the hydrodenitrogenation of pyridine was investigated in an atmospheric-pressure microreactor. The test catalysts consisted of nonsulfided Mo oxide supported on Al_2O_3, SiO_2, and silica–aluminas, containing different concentrations of Mo CUS and Brønsted acidic sites. The kinetic study revealed that Mo loading and support composition affect the specific activity of Mo and selectivity of the catalysts. For the range of conditions used in this study (360–420°C, 1 atm H_2, 0.2 mol% pyridine concentration, differential conversion), the most abundant reaction intermediate was *trans*-2-pentene, and the rate-limiting step was the hydrogenation of the ring. Thus, the overall activity was correlated with the concentration of Mo CUS, which are the hydrogenation sites. The yield of denitrogenated product was also correlated with concentration of CUS. The Brønsted acidic sites determined the selectivity towards the observed cracking, isomerization, and alkylation products.

INTRODUCTION

The increasing demand for more efficient and environmentally benign fuels has raised the standards of performance for hydrotreatment catalysts. The removal of sulfur from heterocyclic compounds is better accomplished than that of nitrogen (1) because most attention has been given to the development of catalysts for light petroleum feedstocks. However, the elimination of nitrogen from heavy petroleums and coal liquid fractions of high nitrogen-content is still a challenging task under typical hydrotreatment conditions (2, 3).

Traditional hydrotreatment (HDS and HDN) catalysts are comprised of sulfided oxides of Co–Mo, Ni–Mo, Ni–Co–Mo, and Ni–W supported on mildly acidic γ-Al_2O_3 (2, 4), although several patents claim better activities and hydrogen utilization by using acidic supports (3, 47, 48). In particular, recent commercial catalyst supports have been successfully modified by P promoter (as in Ref. 48), which not only alters the acidic properties of the support but also affects the microstructure of the transition metal oxides and sulfides deposited on it. The complexity added by the P promoter has resulted in an as yet unsolved problem. Lewis *et al.* (49) give evidence of a primarily structural promotion induced by P on the Mo–Co phases, while Morales *et al.* (50) show the formation of acidic heteropoly compounds, affecting the HDS–HDN selectivity of those catalysts. Direct reference to the mechanistic role of the acidic functionalities in HDS and HDN was provided early by Millman *et al.* (5) and more recently by Hadjiloizou *et al.* (51), Lemberton *et al.* (52), Ozkan *et al.* (53), Lott *et al.* (54), and Olson and Sharma (55). These works have employed promoted and sulfided Co- or Ni–Mo catalysts, with the ensuing difficulty of separating the effects of structural promotion from the acidic site function. A more direct examination of the role of acidity in the HDN mechanism, devoid of the complicating factors induced by promoters and sulfide phases, is thus warranted. This task presupposes the availability of a set of well characterized HDN catalysts containing gauged amount of acidity and no promoter nor sulfide phases.

A set of Mo oxide catalysts supported on a series of silica–aluminas has already been produced. Thereafter, the goal of the present work has become to examine in some detail the functions of the coordinative unsaturated sites of Mo (CUS) and Brønsted acidic sites during the HDN reaction of pyridine.

It has been documented (3, 6–15) that the pyridine HDN reaction follows an established sequence of steps—hetereoaromatic ring hydrogenation, followed by cleavage of the saturated ring at one of the C–N bonds, and the subsequent faster elimination of the $-NH_2$ group as NH_3 (2, 16, 17). McIlvried (7) first suggested a simplified pathway, viz., pyridine → piperidine → *n*-pentylamine → *n*-pentane + NH_3. Later, Sonnemans *et al.* (8–10, 16) proposed a more complex network which involved the formation of *N*-pentylpiperidine. This product was the result of disproportionation reactions of saturated intermediates, occurring at 60 atm but not at atmospheric pressure.

The C–N bond cleavage has been suggested to proceed either by a hydrogenolysis route (28) catalyzed by coordinatively unsaturated sites, or by a Hofmann-type elimina-

[1] To whom correspondence should be addressed. E-mail: r0mira01@ulkyvm.louisville.edu.

0021-9517/95 $12.00

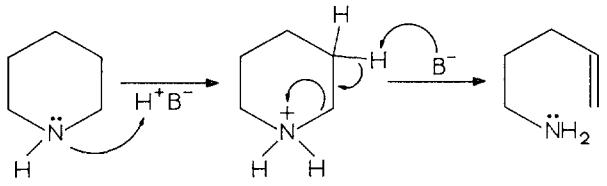

SCHEME 1. Hofmann elimination mechanism as proposed by Nelson and Levy (29).

tion mechanism (29) catalyzed by a Brønsted acid–Lewis base site (Scheme 1). The latter pathway has not been fully demonstrated for Mo catalysts. In this step, piperidine nitrogen is quaternized by the addition of a hydrogen cation from the catalyst surface, while piperidine β-hydrogen cation is abstracted by a surface Lewis base, resulting in C–N bond cleavage. To elucidate the mechanism of C–N bond cleavage by acidic sites, Ledoux and Sedrati (31) examined the piperidine denitrogenation on γ-Al_2O_3 at atmospheric pressure and proved that this reaction can proceed on Brønsted or Lewis acid sites. Ledoux *et al.* also showed that ring opening can occur without complete saturation of pyridine (13). Recently, we have conclusively demonstrated that the piperidine dinitrogenation rate over silica–alumina is directly proportional to the Brønsted acid content (30, 32) in the absence of any hydrogenolysis sites.

Disagreement among different researchers has occurred in regards to the identification of the slow steps in the HDN reaction. Different catalysts and operating conditions have led to differing results. In some instances it has been observed that the pyridine–piperidine reaction attains a thermodynamic equilibrium at normal operating conditions (9, 18–21), suggesting that ring hydrogenation is fast compared to denitrogenation. However, the concensus is that, depending on the catalytic system and process conditions, either the ring hydrogenation (13, 22–25) or the first C–N bond cleavage (7, 19, 26, 27) may be the rate-limiting step.

The specific objective of the present publication is to provide more evidence of how and to what extent Brønsted acidity affects the activity and selectivity of supported Mo oxide catalysts for the HDN of pyridine at atmospheric pressure. The relative importance of each type of functionality (Mo CUS and Brønsted acid sites) is thus investigated, as is the nature of the rate-limiting step under the specified conditions. The catalysts used, containing the two functions, are comprised of nonsulfided molybdena supported on γ-Al_2O_3, SiO_2, and amorphous SiO_2–Al_2O_3.

EXPERIMENTAL

Catalysts

A detailed description of the synthesis of supports, γ-Al_2O_3, SiO_2, and SiO_2–Al_2O_3 (SiO_2:Al_2O_3 = 10:90, 25:75, 50:50, 75:25, and 90:10 wt%), as well as supported Mo catalysts, was reported elsewhere (32, 33). Briefly, alumina was prepared from $Al(NO_3)_3 \cdot 9H_2O$ (Fisher Scientific) and NaOH to obtain a $NaAlO_2$ solution which was precipitated with 3 *N* HNO_3 at 80°C. Silica was synthesized by the addition of 3 *N* HNO_3 to a solution of $Na_2SiO_3 \cdot 9H_2O$ (Fisher Scientific) until a pH of about 3 was achieved. The resultant slurry was neutralized with 6 *N* NH_4OH. The silica–alumina samples were obtained by coprecipitation of the respective precursors. In all cases, the slurry was filtered, dried for 2 h at 110°C, and calcined at 550°C overnight.

The supported MoO_3 catalysts (4, 8, and 12 wt%) were prepared by incipient wetness impregnation using solutions of $(NH_4)_6Mo_7O_{24} \cdot 4H_2O$ (Alfa). The impregnated samples were dried at 120°C for 4 h and calcined in air at 550°C for 12 h. The nomenclature adopted to designate the different supports and catalysts is illustrated in the following examples. SA25 is silica–alumina support containing 25 wt% SiO_2; M8SA25 is 8 wt% MoO_3 on SA25; M8Al and M8Si are 8 wt% MoO_3 on Al_2O_3 and SiO_2, respectively.

These catalysts have previously been characterized by temperature-programmed reduction with H_2, low-temperature oxygen chemisorption (LTOC), NH_3 chemisorption, and temperature-programmed desorption, and infrared spectroscopy of chemisorbed pyridine (32–34). Thus, the amount and type of acidity, as well as the amount of CUS, of the reduced catalysts are known.

Reaction

The reaction was carried out in an atmospheric-pressure microreactor, and the products were analyzed on-line with gas chromatography (Fig. 1) according to a technique described elsewhere (35). All flow rates were regulated with

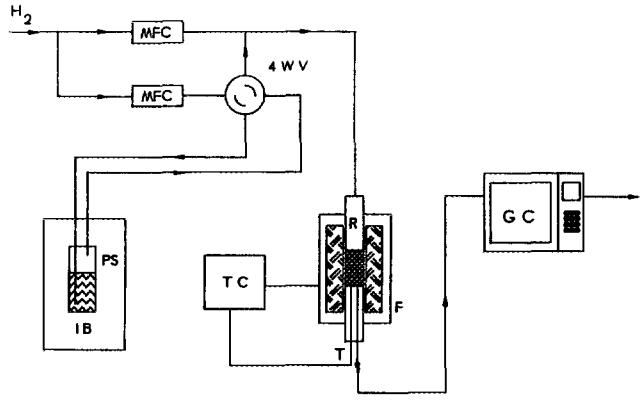

FIG. 1. Experimental setup: (4WV) four-way valve, (MFC) mass flow controler, (PS) pyridine saturator, (IB) ice bath, (R) reactor, (F) furnace, (GC) gas chromatograph, (T) thermocouple, and (TC) temperature controller.

Datametric mass-flow controllers. The reactor consisted of a 5 mm i.d. × 150 mm length quartz tube inserted in an aluminum heating jacket. The catalyst, in the form of 40–60 mesh grains, was supported as a bed between two glass-wool plugs. The temperature was regulated by an Omega temperature controller and monitored by a K-type thermocouple placed in contact with the catalyst bed. The reaction temperatures chosen were 360, 380, 400, and 420°C.

The catalyst loading was varied to keep the mass of Mo constant between runs and equal to 12 mg MoO_3 (e.g., 150 mg of 8% MoO_3). The catalyst was reduced in hydrogen flow (30 ml min^{-1} STP) at 500°C for 4 h. After the reduction step, a four-way valve was switched to allow a stream of hydrogen (10 ml min^{-1} STP) to bubble through a saturator containing pyridine at 0°C, whose purity was verified by GC-MS to be >99.5%. Assuming complete saturation, the pyridine flow rate was calculated to be 2.66 μmol min^{-1}. The pyridine–hydrogen mixture was then diluted with a second hydrogen stream (20 ml min^{-1} STP) and delivered to the reactor through 1.6 mm o.d. stainless steel tubing, which was heated to about 100°C to prevent pyridine condensation. The feed concentration of pyridine was kept constant at about 0.2 mol% and the conversion was kept at differential levels of less than 10% for all experiments. The overall mass balance always closed within ±10%. The absence of mass transfer limitations was confirmed by verifying the independence of measured reaction rate with respect to catalyst particle size (under 30 mesh) and total flow rate (above 20 ml min^{-1} STP) over the temperature range spanned in this study (360–420°C). A measured energy of activation for overall pyridine consumption between 35 and 45 kcal mol^{-1} for the various catalysts reaffirmed the absence of mass transfer limitations. The rates of reaction and product yields reported are those attained after an initial catalyst deactivation and stabilization period of at least 2 days on stream. The runs were repeated several times with fresh loads of catalyst until the reaction rates were reproduced within ±6% deviation.

TABLE 1

Experimental Information and Product Classification

Catalyst load: 12 mg MoO_3 (e.g., 150 mg of 8% MoO_3/support)
Flow rate: 2.66 μmoles of pyridine min^{-1} in balance hydrogen for a total of 30 ml min^{-1} STP
Pressure: slightly above 1 atm
Temperature range: 360–420°C
Conversion of pyridine: less than 10% for all runs

Product classification		
Total products[a]		
HDN		
Cracked C5[b]	Uncracked C5	N-containing
Methane	*trans*-2-Pentene	2-Methyl-pyridine
Ethene	Cyclopentene	4-Methyl-pyridine
Ethane	Cyclopentane	
Propene	1-Pentene	
Propane	*n*-Pentane	
1-Butene		
Isobutene		
trans-2-Butene		
n-Butane		

Note. Definitions: *Conversion of pyridine* = 1 − (exit molar flow-rate of pyridine/inlet molar flow-rate of pyridine); *total products* = HDN products + N-Containing products. (Products are in terms of moles of C5-equivalent, i.e., moles of pyridine converted into products.) *Selectivity to HDN products* = HDN products/total products; *cyclic/saturated* = cyclic C5 product/saturated uncracked C5 product; *saturated/total* = saturated uncracked C5 products/total products; *hydrocracking ratio* = [(C2 + C3) + (C1 + 2C2)]/cracked C5 products; *paraffin/olefin ratio* = paraffin (C2 + C3 + C4 + C5)/olefin (C2 + C3 + C4 + C5) in the HDN products.

[a] The listed products are the only ones detected by FID under the present reaction conditions.

[b] For purposes of mass balance, the four experimental measures of moles of C1, C2, C3, and C4 are arbitrarily grouped into four independent "C5-equivalents": C2 + C3, C1 + 2C2, C1 + C4, and 5C1 (3C1 + C2 and 2C1 + C3 are set = 0).

RESULTS

Table 1 provides a summary of the experimental conditions utilized in this work, as well as a detail of the observed products and pertinent classifications and definitions used in the text. Figure 2 shows the overall reaction rates expressed per unit weight of MoO_3 and as a function of SiO_2 content in the supports. A significant increase in activity occurs for all MoO_3 loadings when the support composition varies between 0 and 100% SiO_2. This is particularly so for the 4 wt% MoO_3 catalysts, which display a fourfold increase, most of it occurring in the range of 50 to 100% SiO_2. The 8 and 12 wt% MoO_3 catalysts show a more modest increase (about twofold) in the same range. There is also a statistically significant *decrease* and minimum in activity observed by the 8 and 12 wt% MoO_3 catalysts in the range of 0 to 75% SiO_2.

These activity profiles may be placed in the context of previous results of characterization by temperature-programmed reduction (TPR), X-ray diffraction (XRD), and infrared spectroscopy of adsorbed pyridine (FTIR), of the oxidic and reduced Mo catalysts (33, 34). The TPR spectra (supported by XRD, Raman, and other spectroscopies, as discussed in Ref. 33) show how the support composition affects the distribution of Mo species and thereby the microstructure and reducibility of the catalysts. Three major types of species dominate; a highly reducible phase of multilayered octahedrally coordinated Mo (whose average

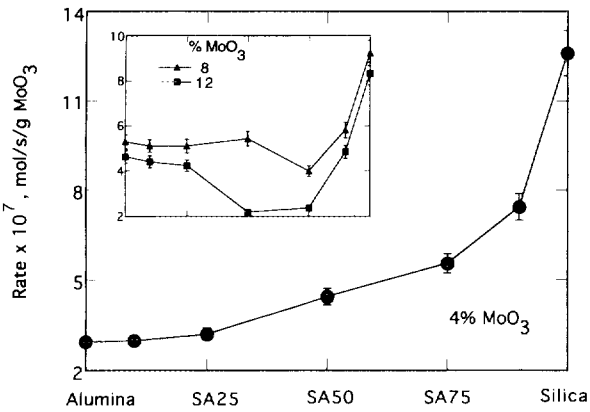

FIG. 2. Overall reaction rate of pyridine at 420°C and 1 atm expressed per g MoO_3 for the three loadings of 4, 8, and 12 wt% MoO_3. The error bars show the standard deviations.

oxidation state may be less than +4 after reduction at 550°C with H_2), a low-reducibility tetrahedrally coordinated Mo (of oxidation state greater than +5), and intermediate-reducibility crystalline phases of orthorhombic MoO_3 and $Al_2(MoO_4)_3$. The relative amounts of these phases at steady state is determined by the density and strength of the basic OH groups originally present in the supports and by the loading of MoO_3. Alumina-rich supports, such as Al_2O_3, SA10, and SA25, loaded up to 4 wt% MoO_3, contain primarily tetrahedrally coordinated Mo oxide. Those supports with higher loadings of MoO_3 contain also multilayers of octahedrally coordinated Mo in proportion to the SiO_2 content. Silica-rich supports, such as SA50, SA75, and SA90, contain mostly octahedrally coordinated Mo and, in the case of SA90, a small amount of orthorhombic MoO_3. SiO_2 support contains mostly orthorhombic MoO_3. The $Al_2(MoO_4)_3$ phase occurs on SA75–SA90 at MoO_3 loading $\geq$8 wt%, but obviously is not present on the SiO_2 support. All of the above species are found in the oxidic form of the catalysts. The chemical properties of the reduced working catalysts depend on the relative amounts of those precursor phases.

The average state of reduction of the catalysts, for example, increases with increasing SiO_2 content in the support and presents a maximum at 75–90% SiO_2 (see Fig. 3). The total acidity, as measured by NH_3 chemisorption, is maximum for catalysts supported on 25% SiO_2 silica–alumina. Lewis as well as Brønsted acidity are present on both the support and the Mo phases under reduced, working conditions. The molar ratio of Brønsted to Lewis acidity presents a maximum at about 75% SiO_2.

Therefore, it is apparent that the activity profiles displayed in Fig. 2 are not determined solely by reducibility nor by type or amount of acidity. In reference to the microstructure of these catalysts (33–34), the activity appears to be better correlated with the relative amount of octahedrally coordinated Mo than with the tetrahedrally coordinated Mo and increases rapidly between 75 and 100% SiO_2, in coincidence with the appearance of orthorhombic MoO_3. This crystalline phase is present in the oxidic form of the catalysts but becomes a denser MoO_2-like structure in the working catalysts (34).

Tables 2–4 present the selectivity to HDN products as defined in Table 1 and the distribution of various HDN products (cracked and uncracked hydrocarbons) as classified in Table 1. The tables also present the calculated values of other parameters which will be used in the discussion.

Pyridine is converted into HDN and N-containing products. The HDN products consist of uncracked C5 and cracked C5 hydrocarbons (i.e., C1–C4), while the N-containing molecules are methyl-pyridines produced by alkylation. In agreement with previous reports of atmospheric HDN of pyridine (9, 14, 15), piperidine and its disproportionation products, such as *N*-pentylpiperidine, are not de-

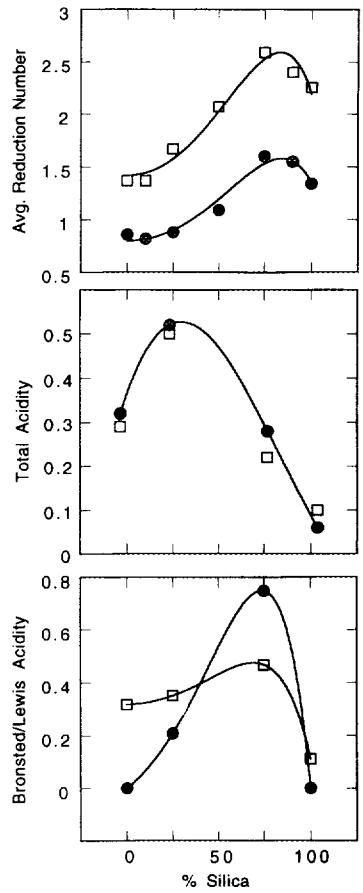

FIG. 3. Properties of the MoO_3 catalysts reduced at 550°C; (top) average reduction number per Mo atom (i.e., loss of oxidation number; e.g., ARN of 2 yields an oxidation number of 6 − 2 = 4); (middle) total acidity, expressed as mmol NH_3/g catalyst; and (bottom) Brønsted/Lewis acidity molar ratio. Loading of MoO_3: (●) 4% and (□) 12%. Adapted from Refs. (33–34).

TABLE 2

Product Distribution for the 4% MoO_3 Catalysts[a]

	Support						
	Alumina	SA10	SA25	SA50	SA75	SA90	Silica
Selectivity to HDN	0.62	0.63	0.64	0.65	0.63	0.66	0.68
Uncracked C5 (%)	55.7	60.0	56.6	59.1	43.8	38.7	33.2
Cracked C5 (%)							
C2 + C3	15.5	14.0	16.3	15.8	20.4	22.4	25.0
C1 + 2C2	0.9	1.3	1.7	1.4	3.0	4.5	4.8
C1 + C4	14.7	12.2	13.6	13.2	17.6	19.1	22.9
5C1	13.2	12.5	11.8	10.5	15.2	15.3	14.1
Cyclic/saturated	0.06	0.09	0.07	0.11	0.07	0.08	0.07
Saturated/total	0.13	0.14	0.13	0.18	0.16	0.18	0.21
Hydrocracking	37.2	38.2	41.4	42.0	41.5	43.8	44.6
Paraffin/olefin	1.12	1.06	1.13	1.21	2.28	3.64	6.19

[a] Reaction conditions: 420°C and 1 atm. Refer to Table 1 for definition of terms.

tected at this pressure. Tables 2–4 reveal that the selectivity to HDN is nearly independent of support composition for SiO_2 <75%, and rises between 75 and 100% SiO_2 in a similar fashion to overall rate of reaction (Fig. 2). Likewise, the selectivity is best for the 4 wt% MoO_3 catalyst and is worse at the higher MoO_3 loadings. For example, the average selectivity for the 4, 8, and 12% MoO_3 catalysts is 0.64, 0.60, and 0.51, respectively.

The hydrogenation activity of the catalysts can be qualified in terms of the ratio of saturated uncracked C5 products to total amount of products, shown in Tables 2–4 as the saturated/total parameter. This remains approximately constant for all support compositions, averaging 0.16, 0.16, and 0.14, respectively, for the 4, 8, and 12% MoO_3 catalysts. The fraction of saturated uncracked C5 products that is cyclic is quantified in Tables 2–4 as the cyclic/saturated parameter. It is also approximately constant for all support compositions, averaging 0.08, 0.08, and 0.06, for 4, 8, and 12% MoO_3. These observations can be rationalized in terms of a single type of site responsible for hydrogenation, a site whose hydrogenation activity is independent of MoO_3 loading and support composition. In view of the structural information already discussed this evidence thus suggests—supporting prior literature—that the hydrogenation sites consist of Mo CUS.

The hydrocracking activity, which involves not only hydrogenation but also acidic sites, is evaluated by means of parameters associated with the cracked C5 fractions of the product distribution. Tables 2–4 give the percentage of C5 fraction that is cracked and the resulting product distribu-

TABLE 3

Product Distribution for the 8% MoO_3 Catalysts[a]

	Support						
	Alumina	SA10	SA25	SA50	SA75	SA90	Silica
Selectivity to HDN	0.61	0.58	0.61	0.63	0.55	0.60	0.65
Uncracked C5 (%)	53.3	55.6	54.9	50.9	44.9	43.8	37.8
Cracked C5 (%)							
C2 + C3	15.3	14.8	15.4	18.3	18.9	20.0	22.7
C1 + 2C2	1.2	1.5	1.3	2.4	2.4	3.1	4.7
C1 + C4	17.7	14.6	15.6	15.1	15.7	17.7	20.4
5C1	12.5	13.5	12.8	13.3	18.1	15.4	14.4
Cyclic/saturated	0.10	0.09	0.09	0.09	0.05	0.06	0.06
Saturated/total	0.18	0.16	0.17	0.17	0.13	0.15	0.17
Hydrocracking	35.3	36.6	36.9	42.2	38.5	41.1	44.1
Paraffin/olefin	1.26	1.21	1.24	1.68	1.74	2.00	3.29

[a] Reaction conditions: 420°C and 1 atm. Refer to Table 1 for definition of terms.

TABLE 4

Product Distribution for the 12% MoO_3 Catalysts[a]

	Support						
	Alumina	SA10	SA25	SA50	SA75	SA90	Silica
Selectivity to HDN	0.52	0.46	0.44	0.47	0.45	0.56	0.66
Uncracked C5 (%)	51.6	52.4	49.3	47.5	44.1	44.3	35.5
Cracked C5 (%)							
C2 + C3	13.6	12.5	14.2	15.7	16.2	18.2	22.1
C1 + 2C2	0.0	0.5	1.1	1.4	2.2	2.6	6.7
C1 + C4	18.8	15.5	15.3	15.8	15.4	17.5	21.3
5C1	16.0	19.1	20.1	19.6	22.1	17.4	14.4
Cyclic/saturated	0.12	0.07	0.08	0.03	0.03	0.05	0.04
Saturated/total	0.19	0.14	0.15	0.12	0.12	0.13	0.15
Hydrocracking	28.3	27.3	30.1	32.7	33.0	37.4	44.5
Paraffin/olefin	1.18	0.94	1.15	1.17	1.36	1.81	3.24

[a] Reaction conditions: 420°C and 1 atm. Refer to Table 1 for definition of terms.

tion, as a function of support composition and MoO_3 loading. Figure 4 shows, for example, such a distribution for the 4% MoO_3 catalysts in terms of mol% of C5-equivalents, i.e., pyridine converted into the various hydrocarbons. The percentage of the C5 products decreases as they are cracked into C1–C4 products by the acidic catalysts. Hence the yields of C2 + C3, C1 + 2C2, C1 + C4, and 5C1 rise following the rising Brønsted/Lewis ratio of the catalysts. This fact is more obvious for the 5C1 fraction, whose yield profile (Fig. 4) resembles the profile of Brønsted/Lewis acidity (Fig. 3). The high activity shown by the 100% SiO_2-supported catalysts, however, is not accounted for by their acidity but by their hydrogenation activity, which is presumably connected with octahedral Mo and its CUS.

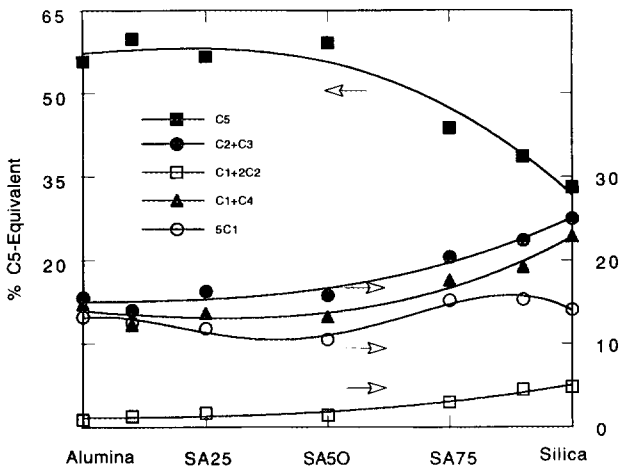

FIG. 4. Distribution of HDN products (hydrocarbons) at 420°C and 1 atm for the 4 wt% MoO_3 catalyst. The cracked HDN products have been regrouped as described in Table 1 in terms of C5-equivalents. The line denoted C5 corresponds to the uncracked C5 products.

Detail about the isomerization selectivity of these catalysts is provided by Figs. 5 and 6. Figure 5 is the distribution of uncracked C5 products as a function of support composition. It is here observed that the majority of C5 consists of *trans*-2-pentene, whose decrease for SiO_2 >50% is due to hydrocracking. *trans*-2-Pentene was the only HDN product detected at low residence time, thus it is a primary product and appears to be a significant intermediate in the mechanism of pyridine HDN at 1 atm. The other isomers become important as the Brønsted acidity and hydrocracking activity of the catalysts increases and *trans*-2-pentene is preferentially cracked to lower hydrocarbons. For example, while the cyclic-C5/*trans*-2-pentene ratio is equal to 0.25 for MoO_3/Al_2O_3, it is equal to 1.5 for MoO_3/SiO_2.

Figure 6 shows the global paraffin/olefin ratio in the cracked and uncracked HDN products, as a function of support composition, MoO_3 loading, and temperature of reaction. This ratio increases with temperature, denoting

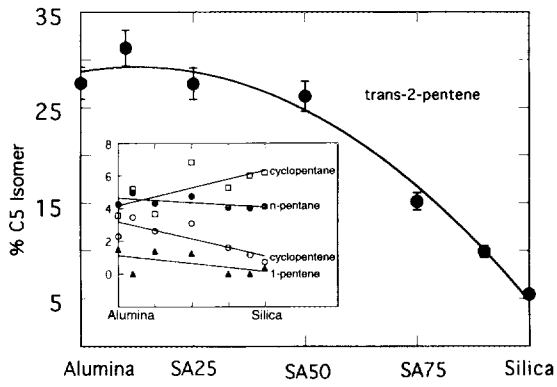

FIG. 5. Distribution of uncracked C5 isomers at 420°C and 1 atm for the 4 wt% MoO_3 catalyst.

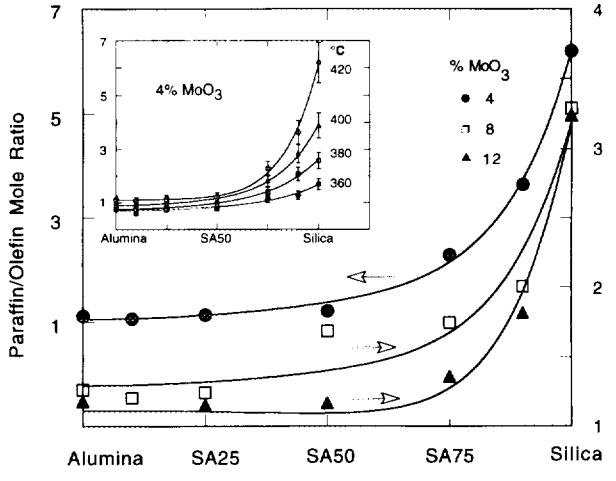

FIG. 6. Paraffin-to-olefin molar ratio at 420°C and 1 atm for the three MoO_3 loadings. The inset shows the ratios for the 4 wt% MoO_3 loading at four temperatures of reaction.

a nonequilibrium, kinetically limited hydrogenation. The ratio has a value of about 1 for all catalysts containing under 50% SiO_2, but increases sharply for SiO_2 >50%, the range in which acidity and hydrocracking activity play a role in the selectivity. The role of this acidity is also seen as the more Brønsted-acidic 4% MoO_3 catalysts achieve greater paraffin/olefin ratio than the 8 and 12% MoO_3 catalysts (for SiO_2 >50%). These observations again indicate that two types of sites are important in determining the selectivity of the catalysts presently studied: Mo CUS and Brønsted acidic sites.

DISCUSSION

The large catalytic activity observed for silica-supported catalysts was unexpected (Fig. 2). Usual reports of rates of hydrotreatment reactions place alumina-supported Mo catalysts above silica-supported catalysts (2, 39–41), but it must be noted, however, that those results are obtained with sulfided Mo oxide catalysts generally in the presence of Co or Ni promoter. In the case of nonsulfided unpromoted Mo oxide catalysts, it appears that SiO_2 support leads to the generation of more active hydrogenation and hydrotreatment sites than Al_2O_3. In such case, the active sites associated with the rate-limiting step are presumably related to Mo CUS, which are more abundant over the SiO_2 support, as will be established in the following discussion.

The evidence presented above suggests that the overall rate of reaction is limited by the rate of hydrogenation of pyridine. Several facts lead to that conclusion. First, the product contains no piperidine, which should have been present if the pyridine hydrogenation reaction was at equilibrium and the piperidine ring opening was the rate-limiting step. Second, rising temperature induces increasing paraffin-to-olefin ratios, which is not consistent with equilibrium but with a kinetically limiting hydrogenation. Therefore, under the present experimental conditions hydrogenation is a slow reaction, and is possibly the rate-limiting step for HDN of pyridine.

It is expected that the more reduced Mo cations are more active for hydrogenation and HDN since they are closer to a metallic state. Such a correlation between rate of benzene hydrogenation and extent of reduction has been found by Yamada *et al.* (42) for Mo over Al_2O_3, but similar work has not been previously reported for SiO_2 or silica–alumina supports. Recently, Rajagopal *et al.* (33) carried out a detailed study of the reducibility of Mo oxide catalysts on silica–aluminas ranging in composition from 0 to 100% SiO_2 (see Fig. 3). They found that under identical reduction conditions, the maximum extent of reduction is attained for Mo on 75% SiO_2. Figure 2, however, reveals that maximum catalyst activity is achieved for 100% SiO_2.

This apparent discrepancy is resolved by considering that the measured extent of reduction includes bulk Mo, therefore, it is not a true measure of the exposed active sites for hydrogenation. The quantity of reduced surface Mo sites can be better approximated by means of LTOC, by assuming that at dry-ice temperature, only one oxygen atom is chemisorbed per reduced site (43, 44). This technique was previously applied to the present catalysts in order to estimate the amount of surface Mo CUS that are generated upon reduction (33 b). It was then found that the concentration of surface CUS is directly proportional to percentage of SiO_2 up to 100%. Figure 7 shows the observed correlation between the overall rate of pyridine reaction and the concentration of CUS for all catalysts and supports considered here. A nonlinear relationship between overall activity and CUS is apparent. Other related works have reported linear correlations between activity and CUS, for example, for thiophene HDS (39, 45, 46) and propylene (44) and hexene hydrogenation (39),

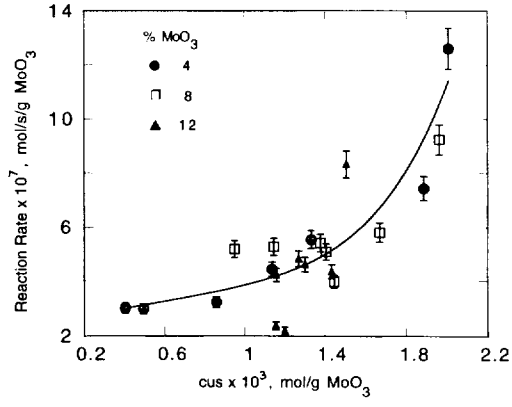

FIG. 7. Overall reaction rate at 420°C and 1 atm as a function of CUS concentration for all catalysts.

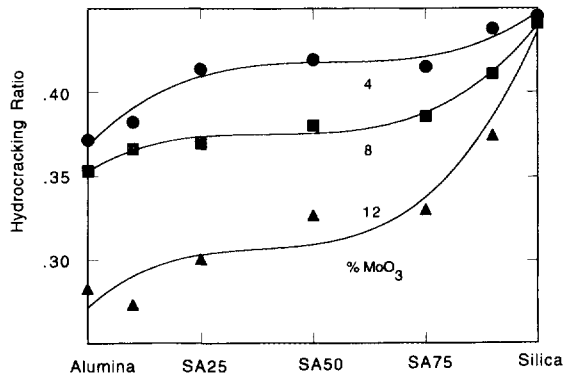

FIG. 8. Selectivity to hydrocracking products at 420°C and 1 atm. Hydrocracking ratio is defined in Table 1.

but those studies did not involve acidic or bifunctional catalysts.

A hypothesis for the nonlinearity in Fig. 7 follows from the arguments and data presented above, although an exhaustive interpretation is beyond the scope of this paper and necessitates further supporting experimentation. Figure 7 can arbitrarily be divided into two regions, roughly below and above 1.2 mmol CUS/g MoO_3. Linear regression of specific rate to CUS concentration in the two regions yields average turnover frequencies of 1.2×10^{-4} and 8.2×10^{-4} s^{-1}, respectively. It must be noted that the higher turnover frequency is for the catalysts containing the higher concentration of CUS and Brønsted acid sites (i.e., for SiO_2 >50%). This is also for those catalysts in which multilayers of octahedrally coordinated Mo and microcrystalline phases of Mo (MoO_3 and $Al_2(MoO_4)_3$) are in appreciable proportion in the precursor materials. Hence, the microstructure of the precursors seem to determine the density of surface CUS in the reduced materials and thereby, possibly through ensemble effects, influence the specific turnover frequency of the sites.

The role of the Brønsted acid sites in affecting the rate of the limiting step for HDN could not be numerically assessed under the present conditions because the rate limiting step preceded the C–N scission step. But the participation of Brønsted acid sites, in cooperation with Mo CUS, is made evident by details of the reaction selectivity. For example, the hydrocracking ratio as defined in Table 1 and shown in Fig. 8, or the C4-to-C3 ratio shown in Fig. 9, are indicators of Brønsted acid site intervention in the mechanism of reaction. It has been demonstrated that hydrogenolysis by metallic sites is preferential toward primary carbons (36, 37) while cracking by acid sites is preferential toward secondary or tertiary carbons (38). Thus it may be assumed that most of C4 products are generated at sites that have metallic character, while C1, C2, and C3 products may arise from both metal and acid-character sites. Thus differences in the hydrocracking ratio should be related to differences in metallic and acidic characters. This is appropriately seen for all catalysts in Fig. 8, which shows significant differences (the error is of the order of symbol size) between the selectivities of the different surfaces. As conceptually necessary, the three curves corresponding to the three MoO_3 loadings converge at the 100% SiO_2 point, since this support favors the formation of the same microcrystalline MoO_3 precursor, regardless of the loading.

The C4-to-C3 ratio (Fig. 9) should in principle increase in direct relation to metallic-to-acidic character of the hydrocracking reaction. As appropriate, higher MoO_3 loading and Al_2O_3 content in the support lead to higher C4-to-C3 ratio, and the minimum ratio is observed roughly about 75% SiO_2, in coincidence with the maximum Brønsted acidity of the catalysts.

Therefore, the information derived from this work leads to the conclusion that mechanisms of pyridine HDN at 1 atm on reduced Mo oxide catalysts should take into account Mo CUS determining the rate of hydrogenation and overall rate of HDN and both Mo CUS and Brønsted acid sites (in cooperation with Lewis basic sites) affecting the hydrocracking reaction selectivity. The primary denitrogenated intermediate is *trans*-2-pentene, which is attainable via C–N hydrogenolysis on Mo CUS or Hofmann elimination on acidic–basic sites. The secondary products are smaller hydrocarbons produced by hydrocracking and alkylated pyridine probably produced by acid-catalysis. The cylic pentane, pentene, and other C5 isomers could be produced by bifunctional catalysis. Scheme 2 illustrates a pathway leading to the *trans*-2-pentene intermediate as well as parallel pathways of denitrogenation by hydrogenolysis and Hofmann elimination.

CONCLUSIONS

The study of pyridine HDN at atmospheric pressure on Mo oxide catalysts supported on silica–aluminas revealed

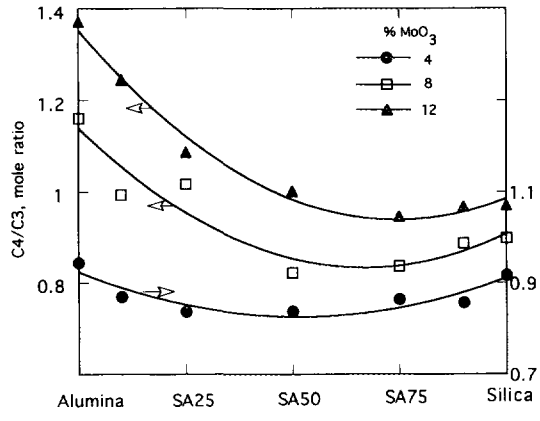

FIG. 9. C4-to-C3 molar ratio obtained on 4 wt% MoO_3 catalysts at 420°C and 1 atm.

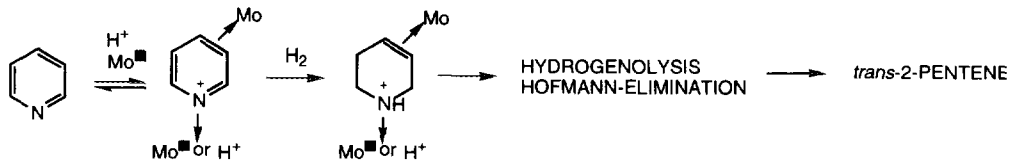

SCHEME 2. A bifunctional model for pyridine adsorption and HDN.

that the hydrogenation activity of Mo CUS determines the overall rate of reaction and that the most likely rate-limiting step is the hydrogenation of the ring. Denitrogenation can occur on both Mo CUS and Brønsted-acid/Lewis-base sites to yield *trans*-2-pentene as a primary intermediate of hydrocracking products. Due to the slow first hydrogenation step, however, the contribution of Brønsted acid sites to the denitrogenation rate cannot be measured under the present conditions. The larger overall rate of reaction observed on silica-supported catalysts than that on alumina-supported ones is thus explained by the larger concentration of Mo CUS on SiO_2 than that on Al_2O_3. The selectivity to various products (C5s, lower hydrocarbons, alkylated pyridines) is determined by the concentration of both Mo CUS and Brønsted acid sites. Therefore, the Mo loading and the support composition, which affect the concentration of those sites, have a significant effect on product selectivity.

ACKNOWLEDGMENTS

We acknowledge the financial support of the Department of Energy (Grant DE-FG22-89PC89771), the National Science Foundation (Grant RII-8610671), and the Commonwealth of Kentucky (EPSCoR Program).

REFERENCES

1. Gates, B. C., Katzer, J. R., and Schuit, G. C. A., "Chemistry of Catalytic Processes." McGraw-Hill, New York, 1979.
2. Katzer, J. R., and Sivasubramanian, R., *Catal. Rev.—Sci. Eng.* **20,** 155 (1979).
3. Ledoux, M. J., *in* "Catalysis, Specialist Periodical Reports" (G. C. Bond and G. Webb, Eds.), Vol. 7, p 125. The Royal Society of Chemistry, London, 1985.
4. Girgis, M. J., and Gates, B. C., *Ind. Eng. Chem. Res.* **30,** 2021 (1991).
5. Millman, W. S., Bartholomew, C. H., and Richardson, R. L., *J. Catal.* **90,** 10 (1984).
6. Ho, T. C., *Catal. Rev.—Sci. Eng.* **30,** 117 (1988).
7. McIlvried, H. G., *Ind. Eng. Chem. Process Des. Dev.* **10,** 125 (1971).
8. Sonnemans, J., and Mars, P., *J. Catal.* **31,** 209 (1973).
9. Sonnemans, J., Van der Berg, G. H., and Mars, P., *J. Catal.* **31,** 220 (1973).
10. Sonnemans, J., Neyens, W. J., and Mars, P., *J. Catal.* **34,** 230 (1974).
11. Fransen, T., van der Meer, O., and Mars, P., *J. Phys. Chem.* **80,** 2103 (1976).
12. Sonnemans, J., Janus, J. M., and Mars, P., *J. Phys. Chem.* **80,** 2107 (1976).
13. Ledoux, M. J., Puges, P. E., and Maire, G., *J. Catal.* **76,** 285 (1982).
14. Ledoux, M. J., *Appl. Catal.* **9,** 31 (1984).
15. Ledoux, M. J., Bouassida, A., and Benazouz, R., *Appl. Catal.* **9,** 41 (1984).
16. Sonnemans, J., and Mars, P., *J. Catal.* **34,** 215 (1974).
17. Shanthi, K., Pillai, C. N., and Kuriacose, J. C., *Appl. Catal.* **46,** 241 (1989).
18. Satterfield, C. N., and Cocchetto, J. F., *AIChE J.* **21,** 1107 (1975).
19. Cocchetto, J. F., and Satterfield, C. N., *Ind. Eng. Chem. Process Des. Dev.* **15,** 272 (1976).
20. Cocchetto, J. F., and Satterfield, C. N., *Ind. Eng. Chem. Process Des. Dev.* **20,** 49 (1981).
21. Hadjiloizou, G. C., Butt, J. B., and Dranoff, J. S., *J. Catal.* **131,** 545 (1991).
22. Moreau, C., and Geneste, P., *in* "Theoretical Aspects of Heterogeneous Catalysis" (J. B. Moffat, Ed.), p. 256. Van Nostrand-Reinhold, New York, 1990.
23. Perot, G., *Catal. Today* **10,** 447 (1991).
24. Kerbeche, A., Hubaut, R., Bonnelle, J. P., and Grimblot, J., *J. Catal.* **131,** 204 (1991).
25. Moreau, C., Aubert, C., Durand, R., Zmimita, N., and Geneste, P., *Catal. Today* **4,** 117 (1988).
26. Satterfield, C. N., and Gultekin, S., *Ind. Eng. Chem. Process Des. Dev.* **20,** 62 (1981).
27. Yang, S. H., and Satterfield, C. N., *Ind. Eng. Chem. Process Des. Dev.* **23,** 20 (1984).
28. Laine, R. M., *Catal. Rev.—Sci. Eng.* **25,** 459 (1983).
29. Nelson, N., and Levy, R. B., *J. Catal.* **58,** 485 (1979).
30. Rajagopal, S., and Miranda, R., *J. Catal.* **141,** 318 (1993).
31. Ledoux, M. J., and Sedrati, M., *J. Catal.* **83,** 229 (1983).
32. Rajagopal, S., Grimm, T. L., Collins, D. J., and Miranda, R., *J. Catal.* **137,** 453 (1992).
33. (a) Rajagopal, S., Marini, H., Marzari, J. A., and Miranda, R., *J. Catal.* **147,** 417 (1994); (b) Miranda, R., Dept. of Energy Reports, Report DOE/PC/89771-13, Nov. 30 (1992).
34. Rajagopal, S., Marzari, J. A., and Miranda, R., *J. Catal.* **151,** 192 (1995).
35. Rajagopal, S., Grimm, T. L., Collins, D. J., and Miranda, R., *Anal. Lett.* **23,** 649 (1990).
36. Gault, F. G., *Adv. Catal.* **30,** 1 (1981).
37. Paäl, Z., *Adv. Catal.* **29,** 273 (1980).
38. Ledoux, M. J., and Djellouli, B. H., *Appl. Catal.* **67,** 81 (1990).
39. Zmierzak, W., Muralidhar, G., and Massoth, F. E., *J. Catal.* **77,** 432 (1982).
40. Duchet, J. C., van Oers, E. M., de Beer, V. H. J., and Prins, R., *J. Catal.* **80,** 386 (1983).
41. Yermakov, Y. I., Startsev, A. N., and Burmistrov, V. A., *Appl. Catal.* **11,** 1 (1984).
42. Yamada, M., Yasumaru, J., Houlla, M., and Hercules, D. M., *J. Phys. Chem.* **95,** 7037 (1991).
43. Parekh, B. S., and Weller, S. W., *J. Catal.* **47,** 100 (1977).
44. Millman, W. S., and Hall, W. K., *J. Catal.* **59,** 311 (1979).
45. Burch, R., and Collins, A., *in* "Proceedings of the 4th International Conference on the Chemistry and Uses of Molybdenum" (H. F. Barry and P. C. H. Mitchell, Eds.), p 379. Climax Molybdenum, Golden, Colorado, 1982.

46. Reddy, B. M., Chary, K. V. R., and Subrahmanyam, V. S., *J. Chem. Soc., Faraday Trans. I* **81,** 1655 (1985).
47. Yamaguchi, E., Uragami, Y., Yokozuka, H., Uekusa, K., Yamaguchi, T., Abe, S., Kamo, T., and Suzuki, T., European Patent Appl. EP 601722 A1 940615, 1994; Nat, P. J., De Booys, J. L., and Schoonhoven, J. W. F. M., European Patent Appl. EP 517300 A1 921209, 1992; Hensley, A. L., Jr., Tait, A. M., Miller, J. T., and Nevitt, T. D., U.S. Patent 4406779 A 830927, 1983.
48. Chao, T. H., U.S. Patent 4629717 A 861216, 1986; Kamo, T., and Kanai, Y., European Patent Appl. EP 496592 A1 920729, 1992.
49. Lewis, J. M., Kydd, R. A., Boorman, M., and Van Rhyn, P. H., *Appl. Catal. A* **84,** 103 (1992).
50. Morales, A., Prada-Silvy, R., and Leon, V., *Stud. Surf. Sci. Catal.* **75** [New Frontiers in Catal., Pt. C], 1899 (1993).
51. Hadjiloizou, G. C., Butt, J. B., and Dranoff, J. S., *Ind. Eng. Chem. Res.* **31,** 2503 (1992).
52. Lemberton, J. L., Gnofam, N., and Perot, G., *Appl. Catal. A* **90,** 175 (1992).
53. Ozkan, U. S., Zhang, L., Ni, S., and Moctezuma, E., *J. Catal.* **148,** 181 (1994).
54. Lott, S. E., Gardner, T. J., McLaughlin, L. I., and Oelfke, J. B., *Prepr. Pap.—Am. Chem. Soc., Div. Fuel Chem.* **39,** 1073 (1994).
55. Olson, E. S., and Sharma, R. K., *Prepr. Pap.—Am. Chem. Soc., Div. Fuel Chem.* **39,** 706 (1994).